Experimental and Computational Studies of the Kinetics and Mechanisms for C_6H_5 Reactions with Acetone-h_6 and -d_6

Y. M. Choi, J. Park, and M. C. Lin*

Department of Chemistry, Emory University, Atlanta, Georgia 30322

Received: January 22, 2003; In Final Form: July 1, 2003

Kinetics and mechanisms for the $C_6H_5 + CH_3C(O)CH_3$ and $CD_3C(O)CD_3$ reactions have been investigated by cavity ring-down spectrometry (CRDS) and hybrid density functional theory (DFT) calculations. The rate constants measured for the two reactions at the constant pressure of 45 Torr using Ar as a carrier gas can be represented by the following Arrhenius expressions in units of $cm^3\ mol^{-1}\ s^{-1}$: $k_H = (4.2 \pm 0.4) \times 10^{11}$ exp[-(955 ± 30)/T] and $k_D = (5.1 \pm 0.6) \times 10^{11}$ exp[-(1114 ± 43)/T] in the temperature ranges of 299−451 and 328−455 K, respectively. The significant kinetic isotope effect observed suggests that H-abstraction is the major path, according to their activation energies, with the $C_6H_5 + CD_3C(O)CD_3$ reaction being higher by 0.3 kcal/mol. DFT calculations at the B3LYP/aug-cc-PVTZ//B3LYP/cc-PVDZ level of theory indicate the reaction can in principle take place by three reaction paths, one H-abstraction and two addition reactions to the C═O double bond at both C and O atom sites, with the latter two processes having significantly higher reaction barriers. The rate constants predicted by canonical variational transition state theory (CVT) with small curvature tunneling (SCT) corrections for the direct H- and D-abstraction reactions are in reasonable agreement with the experimental data after slightly decreasing the calculated barriers from 3.9 kcal/mol to 3.3 kcal/mol and from 4.7 kcal/mol to 4.1 kcal/mol, respectively. The predicted rate constants for $C_6H_5 + CH_3COCH_3$ in the temperature range of 298−1200 K can be represented reasonably by the expression, $k_H = (1.7 \pm 0.6) \times 10^{-1}\ T^{(4.2 \pm 0.1)}$ exp[-(466 ± 26)/T] $cm^3\ mol^{-1}\ s^{-1}$.

I. Introduction

Phenyl radical (C_6H_5) plays a crucial role in the formation of polycyclic aromatic hydrocarbons (PAHs) and soot.[1−6] Kinetics of C_6H_5 reactions with a number of combustion species [7−20] have been measured in this laboratory by the direct detection of the radical with the cavity ringdown spectroscopic (CRDS) method[21] based on the transition first observed by Porter and Ward[22] in 1965. To elucidate the spectroscopic properties of C_6H_5, numerous experimental and theoretical studies have been reported.[9,10,22−31] Experimentally, a series of detailed studies by Radziszewski, Ellison, and co-workers[27−29] reported IR absorption and Raman scattering data. Theoretically, Kim and coworkers[30] assigned the absorption bands of C_6H_5 in ~212, 230−265, and 400−530 nm regions using multireference configuration interaction (MRCI) and complete active space self-consistent field (CASSCF) calculations. Tonokura et al.[31] verified experimentally and computationally the spectral data of Porter and Ward[22] and Yu and Lin[9,10] in the 490−535 nm region.

For the kinetics of C_6H_5 reactions, we have recently extended our studies to include small carbonyl compounds, CH_2O[14,32] and CH_3CHO,[15] both are important combustion intermediates that can be formed by the oxidation of alkyl radicals and unsaturated hydrocarbons. The results of our complementary quantum calculations revealed that the measured low activation energies for these two reactions (E_a < 1 kcal/mol) were dominated by the aldehydic H-abstraction process. Addition reactions to the C═O double bond at both C and O atom sites were found to occur with much higher barriers.[14,15,32] Similarly, for the $C_6H_5 + CH_3CHO$ reaction, H-abstraction from the CH_3-group was concluded to be slow and noncompetitive below 1000 K.[15]

To determine the reactivity of C_6H_5 toward the CH_3-group, we have investigated in this work the kinetics of the reaction with acetone using the same CRDS technique. Similar to the abovementioned aldehyde mechanism, the acetone reaction may occur by a direct H-abstraction and two addition paths

$$C_6H_5 + CH_3C(O)CH_3 \rightarrow C_6H_6 + CH_3C(O)CH_2 \quad (a)$$

$$\rightarrow C_6H_5C(O)(CH_3)_2^{\dagger} \rightarrow C_6H_5C(O)CH_3 + CH_3 \quad (b)$$

$$\rightarrow C_6H_5OC(CH_3)_2^{\dagger} \rightarrow \text{products} \quad (c)$$

where † stands for internal excitation. To examine which reaction path is dominant, we have also investigated the kinetic isotope effect using the fully deuterated acetone, $CD_3C(O)CD_3$. For prediction of rate constants at high temperatures for combustion modeling, we have extrapolated the measured kinetics data with statistical theory calculations based on computed transition state parameters. These results are reported herein.

II. Experimental Measurements

Measurements of the overall rate constants for the C_6H_5 reactions with acetone-h_6 and -d_6 were performed by CRDS under pseudo-first-order conditions with large excess amounts of the molecular reagents at the total pressure of 20−75 Torr using Ar as a carrier gas. The experimental system and procedure employed in this study have been described elsewhere.[10,18]

The cavity length formed by a pair of highly reflective mirrors (R = 0.995 at 500 nm, radius curvature = 6 m) was ap-

* Corresponding author. E-mail: chemmcl@emory.edu.

10.1021/jp0300748 CCC: $25.00
Published on Web 09/04/2003

proximately 500 mm. The phenyl radicals were generated from the photodissociation of C_6H_5NO using the excimer laser (Lambda Physik, LPX 105) operating at 248 nm (KrF); the conversion of C_6H_5NO at this wavelength with an unfocused photolysis laser beam was typically in the range of 8−12%. The probing laser (Lambda Physik, FL 3002) pumped by the pulsed excimer laser (Lambda Physik, EMG201 MSC) generating 308 nm (XeCl) was used for the detection of the phenyl radical at 504.8 nm.[9,10,31] The two lasers controlled by a pulse/delay generator (SRS, DG 535) interfaced with a personal computer by means of the LabVIEW program[33] were operated typically at a repetition rate of 2 Hz to allow for replenishment of the reactants. Decay signals of the probing photon were detected by a photomultiplier tube (Hamamatsu, R955) through a focusing lens and a diffuse glass. The decay signals from the detector were sent to a digitizing oscilloscope (LeCroy, LS140) and then transferred to the computer for further processing. A calibrated K-type thermocouple (Alumel−Chromel) located below the center of the probe region was utilized to measure temperature maintained within ± 0.4 K.

All experiments were carried out under slow-flow conditions. Mixing of reactants and the argon carrier gas was achieved in a stainless bellows tube prior to the introduction into the reactor. Nitrosobenzene was placed on a sealed, fritted glass disk and carried into the reactor via a mixing tube with Ar carrier gas. The initial concentration of C_6H_5NO was determined by standard calibration mixtures to be in the range of $1-8 \times 10^{-11}$ mol cm^{-3} using a UV/VIS spectrometer (SHIMADZU, UV-2401 PC). The concentration of each individual species was obtained by the following formula: $[R] = (\%)\, PF_R / F_T$ Torr, where % is the percentage of the species in its gas mixture, P is the total reaction pressure in Torr, F_R is the flow rate of each gas mixture, and F_T is the total flow rate of all gases. The flow rates were measured by using a mass flowmeter (MKS, 0258C) and the gas pressure was measured with an MKS Baratron manometer.

$CH_3C(O)CH_3$ (Fisher Chemicals, 99.6%) and $CD_3C(O)CD_3$ (Aldrich, 99.5 atom % D) were purified by means of the freeze−pump−thaw degassing procedure with liquid nitrogen (77K) before mixing with argon (Specialty Gases, 99.995% UHP grade) in a concentration of approximately 10% and stored in glass bulbs for kinetic measurements. C_6H_5NO (Aldrich, 97%) was obtained from Aldrich and purified by recrystallization using ethanol as solvent[7] with subsequent vacuum distillation to remove the solvent.

The measured values of photon decay times t_c and t_0 with and without absorbing species are much smaller than the chemical decay time of the radical, t.[9] The following kinetic relationship[7] holds

$$1 / t_c = 1 / t_0 + (cl\,\epsilon / nL)[C_6H_5]_t \qquad (1)$$

or

$$\ln(1 / t_c - 1 / t_0) = B - k_{\text{first}}\, t \qquad (2)$$

where c is the velocity of light, l is the length of the absorbing medium, ϵ is the extinction coefficient, n is the refractive index of the medium, L is the length of the cavity, $[C_6H_5]_t$ is the concentration of the phenyl radical at time t, and $B = \ln\{(cl\epsilon/nL)[C_6H_5]_0\}$. The photon decay times without absorbing species are typically in the range of 25−40 μs, whereas the chemical decay times of the phenyl radical usually varied from 500 to 3000 μs, which depends on the concentration of the reactants. As depicted in Figure 1, the slope of an $\ln(1 / t_c - 1/t_0)$ versus t plot gives the pseudo-first-order rate coefficient, k_{first}, for the decay of the C_6H_5 radical, in the presence of a specified molecular reactant concentration, [acetone-h_6 or -d_6]. Figure 2 presents typical k_{first} versus [acetone] plots which provide the second-order rate constant, k_{second}, according to the relationship based on $k_{\text{first}} = k_0 + k_{\text{second}} \times$ [acetone], where k_0 is the first-order decay coefficient of the phenyl radical in the absence of the molecular reactant, due primarily to the bimolecular $C_6H_5 + C_6H_5NO$ reaction at lower C_6H_5NO conversions and, to some extents, to the radical recombination reactions ($C_6H_5 + C_6H_5$ and C_6H_5 + NO) at higher conversions, as discussed in the Appendix.

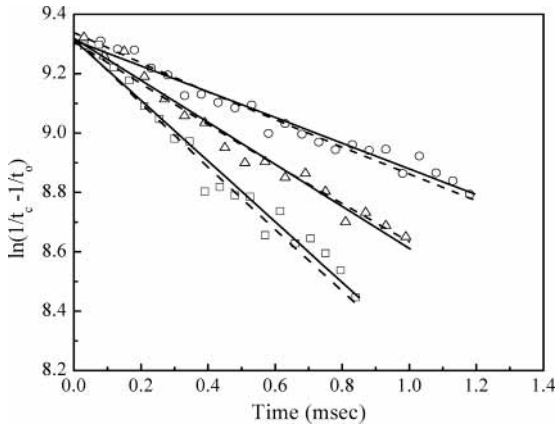

Figure 1. Typical pseudo-first-order plots for the $C_6H_5 + CH_3C(O)CH_3$ reaction against different $CH_3C(O)CH_3$ concentrations: (○), $[CH_3C(O)CH_3] = 0$; (△), $[CH_3C(O)CH_3] = 4.5 \times 10^{-9}$; and (□), $[CH_3C(O)CH_3] = 1.3 \times 10^{-8}$ mol cm^{-3} at $T = 428$ K and $P = 45$ Torr. Solid lines are obtained from linear least-squares analyses; the slopes of these plots give the first-order decay constants, k_{first}. Dashed lines represent modeled C_6H_5 decay plots at the concentration of $CH_3C(O)CH_3$ using the CHEMKIN program**.** The initial concentration of C_6H_5NO is 8.1×10^{-11} mol cm^{-3} with its initial conversion to C_6H_5 estimated to be 14% based on the modeling at $[CH_3C(O)CH_3] = 0$ (see Appendix for explanation on the modeling).

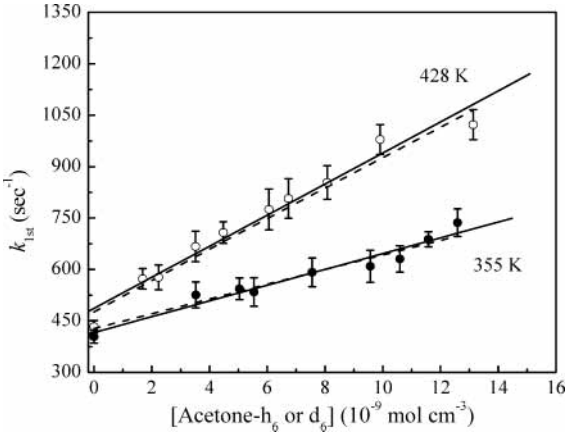

Figure 2. Variation of k_{first} versus acetone concentration for the $C_6H_5 + CD_3C(O)CD_3$ (●) and $CH_3C(O)CH_3$ (○) reactions at 355 and 428 K, respectively. The initial concentrations of C_6H_5NO are 6.5×10^{-11} and 8.1×10^{-11} mol cm^{-3}, with their initial conversions at 10% and 14%, respectively, based on the modeling. Solid and dashed lines are obtained from linear least-squares analyses and modeling, respectively. The linear least-squares fits yield the second-order rate constants.

III. Computational Methods

All electronic structure calculations were performed with the Gaussian 98 program package.[34] All geometries were fully optimized by using the hybrid density B3LYP functional theory[35−37] with the cc-PVDZ basis set of Dunning and co-

TABLE 1: Measured Rate Constants in 10^{10} cm^3 mol^{-1} s^{-1} for the $C_6H_5 + CH_3C(O)CH_3$ and $CD_3C(O)CD_3$ Reactions at Different Temperatures Studied

$C_6H_5 + CH_3C(O)CH_3$			$C_6H_5 + CD_3C(O)CD_3$		
T (K)	$[CH_3C(O)CH_3]$ (Torr)	k_{second}[a]	T (K)	$[CD_3C(O)CD_3]$ (Torr)	k_{second}[a]
299	0−0.19	1.68 ± 0.05	328	0−0.37	1.68 ± 0.18
304	0−0.24	2.02 ± 0.25	355	0−0.28	2.21 ± 0.19
312	0−0.29	2.08 ± 0.10	388	0−0.38	2.98 ± 0.40
324	0−0.21	2.07 ± 0.25	405	0−0.34	3.26 ± 0.24
324	0−0.28	2.31 ± 0.10	455	0−0.31	4.20 ± 0.64
344[b]	0−0.11	2.49 ± 0.19			
344	0−0.23	2.71 ± 0.20			
344[c]	0−0.38	2.78 ± 0.13			
357	0−0.31	2.85 ± 0.39			
392	0−0.23	4.03 ± 0.48			
403	0−0.28	3.68 ± 0.18			
407	0−0.17	4.16 ± 0.30			
428	0−0.35	4.56 ± 0.28			
451	0−0.30	5.08 ± 0.19			

[a] The experimental uncertainties represent 1σ's, evaluated by convoluting errors in the k_{first} determinations using the weighting factor $\omega_i = (k_i/\sigma_i)^2$ (ref 44). [b] P =20 Torr. [c] P = 75 Torr; otherwise, P = 45 Torr.

workers[38,39] according to the Berny algorithm.[40] For transition state searches, we applied the Synchronous Transit-Guided Quasi-Newton (STQN) method.[40,41] Intrinsic reaction coordinate (IRC)[42,43] calculations were then carried out to confirm the connection between each transition state and designated reactants and products. Harmonic vibrational frequencies calculated at the B3LYP/cc-PVDZ level of theory were used for zero-point energy (ZPE) corrections and rate constant calculations. Energies for the construction of potential energy surface (PES) and the prediction of reaction rate constants were further calculated at the B3LYP/aug-cc-PVTZ level based on the optimized geometries at the B3LYP/cc-PVDZ level of theory.

IV. Results and Discussion

A. Kinetic Data Analysis. Table 1 gives all of the rate constants obtained by CRDS at the total pressure of 20−75 Torr and the repetition rate of 2 Hz. As represented in Figure 2, the pseudo-first-order rate coefficient (k_{first}) varied with molecular concentrations and the second-order rate constant k_{second} was obtained from the slope. Least-squares analyses of the absolute rate constants for the $C_6H_5 + CH_3C(O)CH_3$ and $D_3C(O)CD_3$ reactions in the temperature ranges of 299−451 K and 328−455 K, respectively, can be represented by the Arrhenius equations in units of cm^3 mol^{-1} s^{-1}

$$k\,(C_6H_5 + CH_3COCH_3) = (4.2 \pm 0.4) \times 10^{11} \exp[-(955 \pm 30)/T]$$

$$k\,(C_6H_5 + CD_3COCD_3) = (5.1 \pm 0.6) \times 10^{11} \exp[-(1114 \pm 43)/T]$$

where the error limits represent 1σ's, evaluated by convoluting errors in the k_{first} and k_{second} determinations using the weighting factor $\omega_i = (k_i/\sigma_i)^2$.[44] Although the reactions can take place by many paths as alluded to in the Introduction, the significant kinetic isotope effect (see Figure 3) suggests that the H-abstraction is the major path according to their activation energies, with the $C_6H_5 + CD_3C(O)CD_3$ reaction being higher by 0.3 kcal/mol.

We have examined the possible effects of pressure and photolysis laser energy. The variation of total pressure between 20 and 75 Torr led to no noticeable effect within the scatter of the data (see Figure 3). Similarly, an increase in the photolysis laser energy from 20 to 48 mJ gave rise to no systematic variation in the measured and kinetically modeled bimolecular rate constant as illustrated in the Appendix. Kinetic modeling was carried out with the CHEMKIN[45] program using the mechanism presented in Table A1. Such modeling allows us to simulate the observed C_6H_5 radical decay rates by CRDS with and without the molecular reactant and the dependence of photolysis laser power, or lack of it, as illustrated in the Appendix. In Figures 1 and 2, the dashed lines represent kinetically modeled values; the pseudo-first-order decay kinetics and the linear dependence of k_{first} on the molecular reactant concentration can be quantitatively simulated.

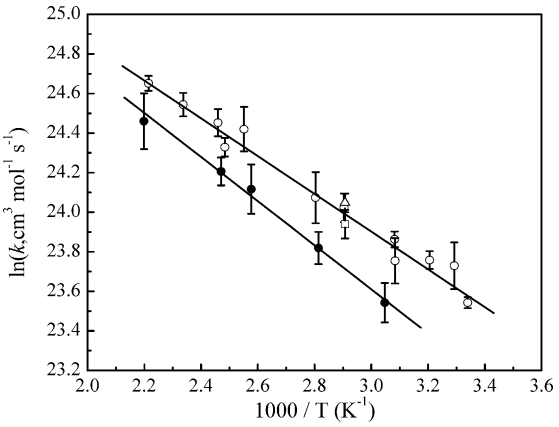

Figure 3. Arrhenius plots of overall rate constant for the $C_6H_5 + CH_3C(O)CH_3$ reaction (○) and the $C_6H_5 + CD_3C(O)CD_3$ reaction (●). Solid lines represent the results of least-squares analyses with convolution of errors in k_{first}. (□) and (△) correspond to the experimental results at 20 and 75 Torr, respectively.

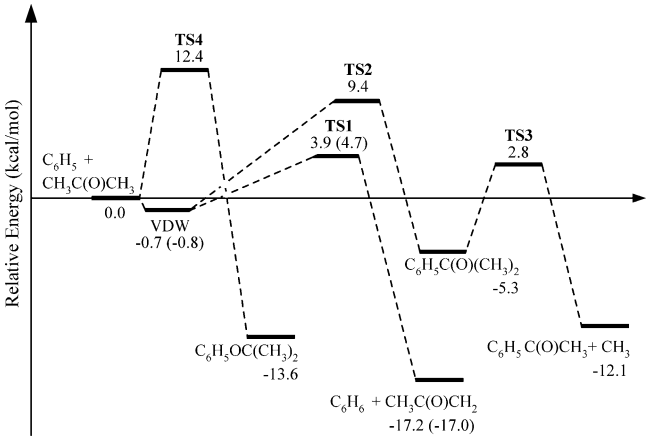

Figure 4. Schematic energy diagram for the $C_6H_5 + CH_3C(O)CH_3$ reaction calculated at the B3LYP/aug-cc-PVTZ//B3LYP/cc-PVDZ level of theory. The relative energies of the direct abstraction reaction through **TS1** in parentheses are for the $C_6H_5 + CD_3C(O)CD_3$ reaction.

B. Reaction Mechanism. As described in the Introduction, the reaction of C_6H_5 with $CH_3C(O)CH_3$ can occur via three reaction paths, a H-abstraction reaction and two addition reactions. Figure 4 depicts the schematic energy diagram of the reaction calculated at the B3LYP/aug-cc-PVTZ//B3LYP/cc-PVDZ level of theory.

For the direct H-abstraction reaction a, it takes place by C_6H_5 approaching one of the six hydrogen atoms of the two methyl groups through a weakly bonded complex found by IRC analysis. After overcoming **TS1** with a barrier of 3.9 kcal/mol, reaction a directly gives the products, C_6H_6 and acetonyl radical (CH_3COCH_2), with a predicted exothermicity of 17.2 kcal/mol.

TABLE 2: Unscaled Vibrational Frequencies and Moments of Inertia for the Species Involved in the Direct Abstraction Pathways for the C_6H_5 + $CH_3C(O)CH_3$ and $CD_3C(O)CD_3$ Reactions Computed at the B3LYP/cc-PVDZ Level of Theory

species	I_A, I_B, I_C (10^{-40} g cm^2)	υ_i (cm^{-1})
C_6H_5	134.3,150.5,284.8	402,425,597,614,673,721,815,893,967,981,998,1022,1047,1070,1164,1165,1292, 1340,1457,1465,1584,1639,3163, 3170,3182,3185,3196
$CH_3C(O)CH_3$	83.2,99.2,171.9	43,147,377,489,531,789,869,880,1071,1104,1229,1361, 1370,1427,1435,1438,1458, 1812,3026,3033,3090,3097, 3152,3152
$CD_3C(O)CD_3$	99.9,131.9,210.8	31,109,316,404,477,661,694,708,889,974,1001,1027,1031,1037,1050,1089,1251, 1805,2175,2180,2285,2291,2335, 2338
TS1-h_6	300.7,1416.9,1561.3	1078*(i)*,26,35,46,91,132,136,365,394,404,426,505,540, 576,608,670,720,735, 807,840,902,917,932,979,1007,1008,1034,1065,1077,1080, 1083,1167,1173,1239,1301,1308, 1341,1364,1378,1425,1436,1448,1466, 1487,1601,1636,1762,3028,3083,3093,3152,3164,3171,3175,3181,3187, 3196
TS1-d_6	333.6,1509.8,1645.4	804*(i)*,24,33,44,87,97,130,302,352,395,404,446,468,493, 607,682,691,696,715, 731,741,840,885,912,936,949,979, 987,1004,1007,1013,1029,1033, 1043,1066,1080,1096,1167,1173,1263,1309,1343,1460,1483,1598, 1635,1754, 2176,2237,2287,2336,2360,3163,3171,3180,3187,3196
C_6H_6	148.1,148.1,296.2	414,414,618,618,692,723,866,866,987,987,1014,1019, 1022,1059,1059,1162,1187, 1187,1357,1365,1507,1507, 1646,1646,3163,3174,3174,3190,3190,3201
C_6H_5D	148.1,158.4,306.5	392,414,611,614,621,718,796,864,866,944,987,1000,1013,1017,1056,1100,1172, 1187,1334,1358,1479,1501,1640, 1641,2352,3166,3174,3182,3190,3198
$CH_3C(O)CH_2$	77.1,93.1,164.9	71,370,383,507,523,745,823,919,1013,1056,1263,1370, 1430,1448,1449,1602, 3032,3097,3139,3152,3264
$CD_3C(O)CD_2$	90.8,120.1,200.3	51,266,319,424,468,597,705,757,874,890,1014,1033,1043,1102,1299,1593,2179, 2275,2291,2336,2434

The D-abstraction reaction has a slightly higher barrier with 4.7 kcal/mol (see Figure 3). For the addition reaction b, the first step is the formation of $C_6H_5C(O)(CH_3)_2$ with an exothermicity of 5.3 kcal mol^{-1} after overcoming **TS2** with a reaction barrier of 9.4 kcal/mol. The adduct can then undergo decomposition by eliminating one of the two methyl groups via a 2.8 kcal/mol barrier at **TS3** with an overall exothermicity of 12.1 kcal/mol.

For reaction c, the C atom of the phenyl radical can add to the O atom of the C═O group via **TS4** with a reaction barrier of 12.4 kcal/mol. It forms the radical adduct, phenoxy-isopropyl, with a 13.6 kcal/mol exothermicity. For this pathway, we did not search further for additional reaction products on account of the high barrier; it is kinetically unfavorable.

C. Rate Constant Calculations. The rate constant for the dominant H-abstraction reaction was computed with the Polyrate program.[46] The rate constants for the addition reactions are estimated to be several orders of magnitude smaller than that of the H-abstraction reaction based on the reaction barriers shown in Figure 4. The optimized geometries of the reactants, products, and transition state for the hydrogen abstraction reaction are presented in Figure 5. Table 2 gives harmonic vibrational frequencies and moments of inertia for the species involved in the direct abstraction reactions.

Treatment of Torsional Motions in Acetone. The simplest molecule[47] that has two methyl groups with C_{3v} rotor is ethane (CH_3CH_3) with the torsional frequency of 289 cm^{-1},[48] whose approximated value at the B3LYP/cc-PVDZ level of theory is 318 cm^{-1}. The potential curve of the hindered rotation in ethane can be obtained by rotating one of the methyl groups with a relaxed optimization method. On the other hand, $CH_3C(O)CH_3$ with C_{2v} symmetry has two torsional vibrations owing to the presence of the carbonyl group. Thus, to treat the torsional motions of acetone, we carried out one-dimensional hindered rotation at the B3LYP/cc-PVDZ level of theory: the dihedral angle, ∠OCCH (see Figure 5), of one of the methyl groups was varied with the fully relaxed optimization method to produce a torsional barrier of 266 cm^{-1}. It should be noted that the two parameters for the Polyrate program,[46] P, the number of distinct minima, and σ_1, symmetry number of a minimum, are 1 and 3, respectively. Two vibrational frequencies of υ_1 and υ_2 were

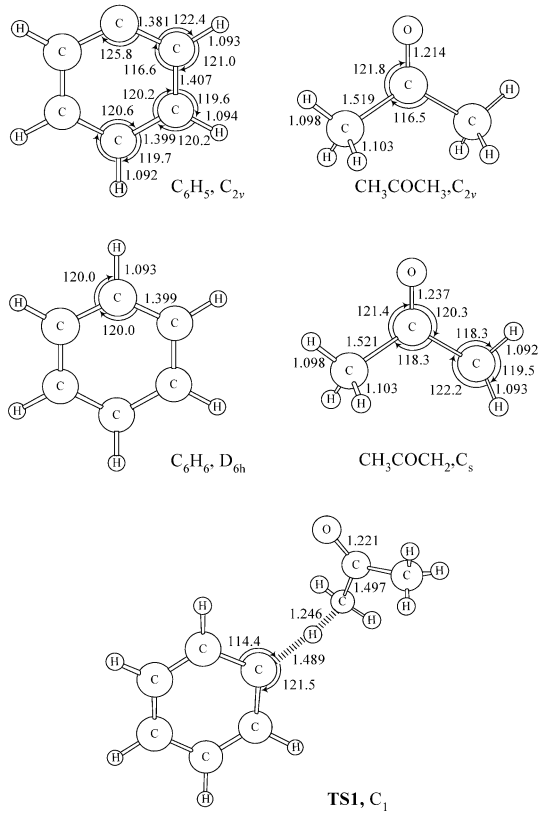

Figure 5. Optimized structures of the reactants, transition state, and products for the direct H-abstraction reaction for the C_6H_5 + $CH_3C(O)CH_3$ reaction at the B3LYP/cc-PVDZ level of theory. Bond lengths are in Å and bond angles are in degrees.

treated by the hindered-internal-rotor approximation.[49] To approximate the reduced moment of inertia for the torsional motions, scheme Cw[49] based on a curvilinear model was chosen. In the scheme Cw, the following relationship holds:[49]

$$W_j = 2\, I_j\, (w_j / M)^2 \qquad (3)$$

where W_j is the torsional barrier and I_j is the moment of inertia for the jth internal rotation, w is the harmonic frequency, and

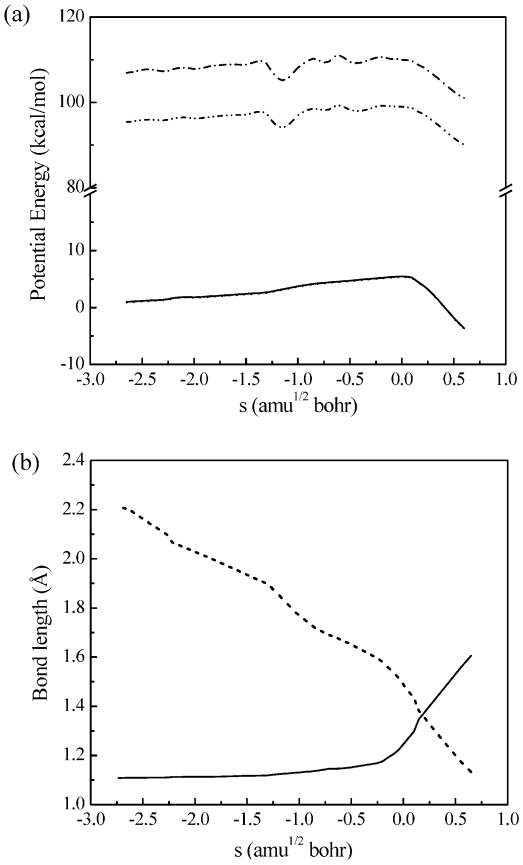

Figure 6. (a) Classical potential energy and vibrationally adiabatic ground-state potential energy curves versus mass-weighted reaction coordinate (s; amu$^{1/2}$ bohr) for the direct abstraction reactions of the $C_6H_5 + CH_3C(O)CH_3$ and $CD_3C(O)CD_3$ reactions. Solid line corresponds to the classical potential energy for $C_6H_5 + CH_3C(O)CH_3$ and dotted line to that for $C_6H_5 + CD_3C(O)CD_3$. Dashed−dotted line corresponds to the vibrationally adiabatic ground-state potential energy for $C_6H_5 + CH_3C(O)CH_3$ and dashed−dotted-dotted line to that for $C_6H_5 + CD_3C(O)CD_3$. (b) Variations of main geometrical parameters along the MEP. Solid line represents the distance of $CH_3C(O)CH_2\cdots H$ and dotted line shows that of $H_5C_6\cdots H$.

M is the total number of minima along the coordinate from 0 to 360° with $j = 1, 2,..., P$.

CVT Predictions. For the $C_6H_5 + CH_2O$ and CH_3CHO reactions, both occurring with small barriers (<1 kcal/mol), we reported[14,32] that canonical variational transition state theory (CVT)[50] reproduced more accurately experimental data than did the conventional transition state theory with Eckart tunneling corrections. In this work, for the CVT calculation using the Polyrate program,[46] the direct H-abstraction pathway forming C_6H_6 and $CH_3C(O)CH_2$ has been mapped out following the minimum energy path (MEP) with the tight convergence criterion at the B3LYP/cc-PVDZ level of theory. Projected frequency calculations[51] were then performed at thirty points along the MEP. The electronic energy at each point was scaled and adjusted based on the single-point energy from the B3LYP/aug-cc-PVTZ level of theory. Figure 6a shows the classical potential curve, $V_{MEP}(s)$, without zero-point corrections and the vibrationally adiabatic ground-state potential energy curve, $V_A^G(s)$. Figure 6b presents the variation of main geometrical parameters along the MEP in which negative and positive directions correspond to the reactant and product sides, respectively. The forming C−H distance of $H_5C_6\cdots H$ decreases over the reaction coordinate. The breaking C−H distance of $CH_3C(O)CH_2\cdots H$ has no apparent variation before approximately *s* = −0.4 amu$^{1/2}$ bohr. Then, it elongates linearly and proceeds to separate the bond up to 1.606 Å forming the acetonyl radical.

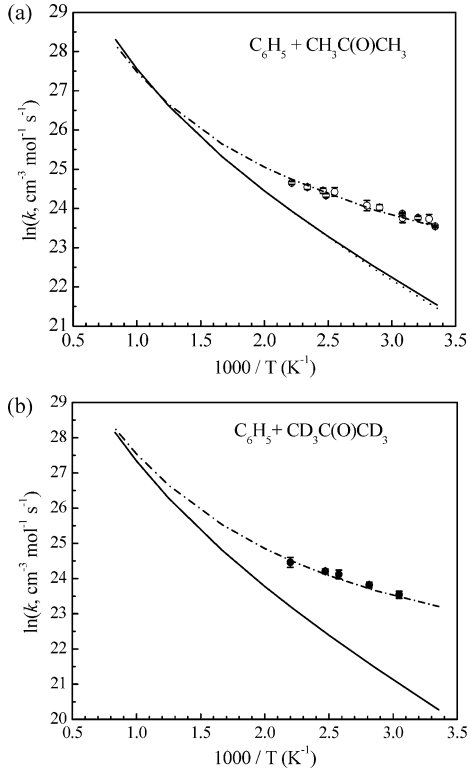

Figure 7. (a) Comparison of the experimental and predicted rate constants of the H-abstraction reaction in $C_6H_5 + CH_3C(O)CH_3$. Open circle (○), experimental data; solid line, standard TST prediction; dotted line, CVT prediction; and dash−dotted, CVT/SCT prediction with $E_0 = 3.3$ kcal/mol. (b) Arrhenius plots for the D-abstraction reaction of the $C_6H_5 + CD_3C(O)CD_3$ reaction. Open circle (●), experimental data; solid line, standard TST prediction; dotted line, CVT prediction; and dash−dotted, CVT/SCT prediction with $E_0 = 4.1$ kcal/mol.

As aforementioned, two harmonic vibrational frequencies of ν_1 and ν_2 for acetone were treated as hindered rotors with $P = 1$ and $\sigma_1 = 3$. However, ν_2 and ν_6 of **TS1** were treated approximately as free rotors contributing by the C_6H_5 and CH_3 rotations, respectively. To treat those vibational frequencise as free rotors, torsional barriers for the motions were made to be very small ($W_m \approx 0$).[52]

Figure 7 shows the comparisons of the experimental data with the predicted ones by TST, CVT, and CVT/SCT, for the direct abstraction reactions. For the acetone-h_6 reaction, it is apparent that there is a very small variational effect at low temperatures. However, no such variational effect is noted in the acetone-d_6 reaction. Figure 7a presents the rate constants from CVT/SCT for the acetone-h_6 reaction after decreasing the barrier height obtained from B3LYP/aug-cc-PVTZ//B3LYP/cc-PVDZ, 3.9 kcal/mol, to 3.3 kcal/mol to fit our experimental data. The CVT/SCT rate constant for the acetone-d_6 reaction also gave a good agreement with the same shift energy of 0.6 kcal/mol from 4.7 kcal/mol to 4.1 kcal/mol. The predicted rate constants compiled in Table 3 can be recommended for kinetic modeling in the temperature range of 298−1200 K, with the following expressions given in units of cm^3 mol^{-1} s^{-1}:

$$k = (1.7 \pm 0.6) \times 10^{-1}\, T^{(4.2 \pm 0.1)} \times \exp[-(466 \pm 26)/T] \text{ for } C_6H_5 + CH_3C(O)CH_3$$

$$k = (6.4 \pm 2.7) \times 10^{-3}\, T^{(4.6 \pm 0.1)} \times \exp[-(546 \pm 31)/T] \text{ for } C_6H_5 + CD_3C(O)CD_3$$

TABLE 3: Predicted Rate Constants (cm^3 mol^{-1} sec^{-1}) for the Direct Abstraction Processes in the $C_6H_5 + CH_3C(O)CH_3$ and $CD_3C(O)CD_3$ Reactions

	$C_6H_5 + CH_3C(O)CH_3 \rightarrow C_6H_6 + CH_3C(O)CH_2$		$C_6H_5 + CD_3C(O)CD_3 \rightarrow C_6H_5D + CD_3C(O)CD_2$	
T (K)	CVT	CVT/SCT	CVT	CVT/SCT
298	2.07×10^9	1.66×10^{10}	6.37×10^8	1.20×10^{10}
300	2.16×10^9	1.68×10^{10}	6.72×10^8	1.22×10^{10}
350	5.71×10^9	2.56×10^{10}	2.12×10^9	1.89×10^{10}
400	1.28×10^{10}	3.90×10^{10}	5.29×10^9	2.88×10^{10}
450	2.41×10^{10}	5.51×10^{10}	1.12×10^{10}	4.28×10^{10}
500	4.13×10^{10}	7.60×10^{10}	2.11×10^{10}	6.21×10^{10}
600	9.94×10^{10}	1.37×10^{11}	5.90×10^{10}	1.22×10^{11}
800	3.60×10^{11}	3.77×10^{11}	2.59×10^{11}	3.75×10^{11}
1000	9.24×10^{11}	8.59×10^{11}	7.41×10^{11}	9.11×10^{11}
1200	1.94×10^{12}	1.71×10^{12}	1.67×10^{12}	1.88×10^{12}

V. Conclusions

The reactions of phenyl radicals with acetone-h_6 and -d_6 have been investigated by CRDS and the hybrid density functional B3LYP method. The overall rate constants were measured mostly at the total pressure of 45 Torr using C_6H_5NO as the C_6H_5 radical source with argon as the carrier gas. Least-squares analyses of the rate constants obtained from the experiment gave the following expressions in units of cm^3 mol^{-1} s^{-1}; k ($C_6H_5 + CH_3COCH_3$) = $(4.2 \pm 0.4) \times 10^{11}$ exp[$-(955 \pm 30)$ / T] and k ($C_6H_5 + CD_3COCD_3$) = $(5.1 \pm 0.6) \times 10^{11}$ exp[$-(1114 \pm 43)$ / T] in the temperature ranges of 299−451 K and 328−455 K, respectively. No noticeable effect with total gas pressure was found in the rate constant determination. The rate constants predicted by canonical variational transition state theory with small curvature tunneling corrections for the direct abstraction of H and D are in good agreement with the experimental data after slightly adjusting the calculated barrier heights at the B3LYP/aug-cc-PVTZ//B3LYP/cc-PVDZ level of theory. Other product channels occurring via addition to the C═O bond were calculated to be unimportant kinetically.

Acknowledgment. The authors are grateful for the support of this work from the Basic Energy Sciences, Department of Energy, under contract no. DE-FG02-97-ER14784. Our thanks go to Prof. D. Truhlar of University of Minnesota for the use of the Polyrate program and to the Cherry L. Emerson Center of Emory University for providing its resources, which are in part supported by a National Science Foundation grant (CHE-0079627) and an IBM shared University Research Award.

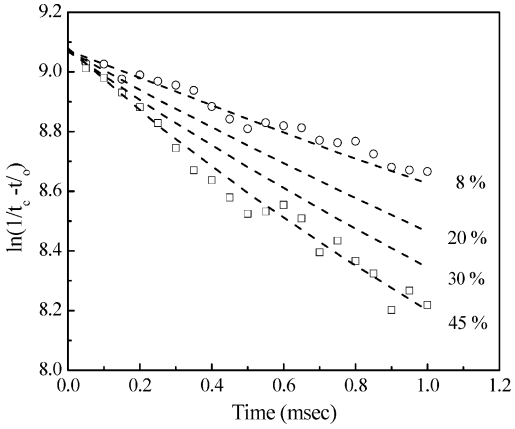

Figure A1. Pseudo-first-order decay plots of C_6H_5 at different photolysis energies: (○) and (□) correspond to the experimental results obtained at 21 and 60 mJ, respectively, at T = 343 K and P = 45 Torr. The dashed lines represent modeled C_6H_5 decay rates at different C_6H_5NO conversions using the CHEMKIN program.

Appendix

Kinetic Modeling of C_6H_5 Radical Decay Rates. The decay of phenyl radicals produced in the photodissociation of C_6H_5-NO in a CRDS cavity can be kinetically modeled using the reaction mechanism summarized in Table A1. As shown in Fig. A1, the decay of phenyl radicals generated by different 248 nm beam energies in the absence of the CH_3COCH_3 reactant, with 8−45% of C_6H_5NO conversions by the 248 nm photons at the initial concentration of 7.0×10^{-11} mol cm^{-3}, varies linearly with time at small conversions (<20%) attributable mainly to the $C_6H_5 + C_6H_5NO$ reaction, whereas at higher

TABLE A1: Reactions and Rate Constants[a] Used in the Modeling of the $C_6H_5 + CH_3C(O)CH_3$ and $CD_3C(O)CD_3$ Reactions in the CRDS Experiment

	reactions	A	n	E_a	ref[b]
1a	$C_6H_5 + CH_3COCH_3 \rightarrow C_6H_6 + CH_3COCH_2$	4.20×10^{11}	0.0	1898	this work
1b	$C_6H_5 + CD_3COCD_3 \rightarrow C_6H_5D + CD_3COCD_2$	5.10×10^{11}	0.0	2214	this work
2	$C_6H_5 + C_6H_5NO \rightarrow C_{12}H_{10}NO$	4.90×10^{12}	0.0	−68	
3	$C_6H_5 + C_6H_5 \rightarrow C_{12}H_{10}$	1.39×10^{13}	0.0	111	
4	$C_6H_5 + NO \rightarrow C_6H_5NO$	2.95×10^{12}	0.0	−860	
5	$C_6H_5NO \rightarrow C_6H_5 + NO$	1.42×10^{17}	0.0	55060	
6	$C_6H_5 + C_{12}H_{10}NO \rightarrow C_6H_5O + C_{12}H_{10}N$	1.00×10^{13}	0.0	0	
7	$C_6H_5 + C_6H_5O \rightarrow C_{12}H_{10}O$	1.39×10^{13}	0.0	111	
8	$C_6H_5 + C_{12}H_{10}N \rightarrow C_{18}H_{15}N$	1.39×10^{13}	0.0	111	
9	$C_6H_5 + C_6H_5NO \rightarrow C_{12}H_{10} + NO$	5.00×10^{12}	0.0	4500	
10	$C_{12}H_{10}N + NO \rightarrow C_{12}H_{10}NNO$	1.00×10^{13}	0.0	0	
11	$C_{12}H_{10}NO \rightarrow C_6H_5NO + C_6H_5$	5.00×10^{14}	0.0	45000	
12	$C_6H_5 + CH_3COCH_2 \rightarrow C_9H_{10}O$	1.00×10^{13}	0.0	0	*c*
13	$2CH_3COCH_2 \rightarrow C_6H_{10}O_2$	1.00×10^{13}	0.0	0	*c*
14	$CH_3COCH_2 + NO \rightarrow CH_3COCH_2NO$	1.00×10^{12}	0.0	0	*c*

[a] Rate constants are defined by $k = AT^n \exp(-E_a / RT)$ and in units cm^3, mol, and s; E_a is in the units of cal/mol. [b] Ref 53 unless otherwise noted. [c] Assumed.

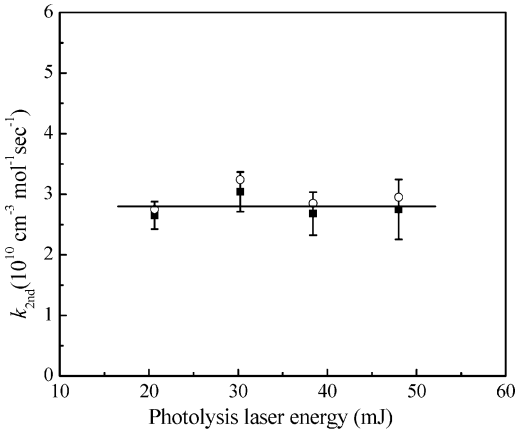

Figure A2. Measured (■) and modeled (○) second-order rate constants for the $C_6H_5 + CH_3C(O)CH_3$ reaction as a function of photolysis laser energy at $T = 343$ K and $P = 45$ Torr.

conversions (>30%) a slight nonlinear decay appears, attributable to the fast radical−radical reactions such as $C_6H_5 + C_6H_5$ and NO based on the result of our sensitivity analysis. Because the key primary C_6H_5 reactions listed in the mechanism had been reliably measured in our previous studies,[19,53] the decay of C_6H_5 radicals measured in the absence of $CH_3C(O)CH_3$ (k_0) in each series of experimental runs provides us a reasonable estimate for the initial averaged concentration of C_6H_5, which in turn allows us to simulate the linear dependence of k_{first} and its dependence on the molecular reactant concentration as illustrated by Figures 1 and 2 presented in the text, and to model the photolysis energy dependence also as shown in Figure A2, which reveals no such dependence within the experimental scatter.

References and Notes

(1) Zhang, H. Y.; McKinnon, J. T. *Combust. Sci. Technol.* **1995**, *107*, 261.
(2) Richter, H. M., O. A.; Sumathi R.; Green, W. H.; Howard. J. B.; Bozzelli J. W. *J. Phys. Chem. A.* **2001**, *105*, 1561.
(3) Haynes, D. S. *Fossil Fuel Combustion*; Wiley-Interscience: New York, 1991.
(4) Bockhorn, H. *Soot Formation in Combustion*; Springer-Verlag: New York, 1993.
(5) Glassman, I. *Combustion*, 2nd ed.; Academic Press: New York, 1986.
(6) Brezinsky, K. *Prog. Energy Combust. Sci.* **1986**, *12*, 1.
(7) Yu, T.; Lin, M. C. *J. Am. Chem. Soc.* **1993**, *115*, 4371.
(8) Yu, T.; Lin, M. C. *J. Phys. Chem.* **1994**, *98*, 7.
(9) Yu, T.; Lin, M. C. *J. Phys. Chem.* **1994**, *98*, 2105.
(10) Yu, T.; Lin, M. C. *J. Am. Chem. Soc.* **1994**, *116*, 9571.
(11) Yu, T.; Lin, M. C. *Int. J. Chem. Kinet.* **1994**, *26*, 771.
(12) Yu, T.; Lin, M. C. *J. Phys. Chem.* **1995**, *99*, 8599.
(13) Yu, T.; Mebel, A. M.; Lin, M. C. *J. Phys. Org. Chem.* **1995**, *8*, 47.
(14) Choi, Y. M.; Xia, W. S.; Park, J.; Lin, M. C. *J. Phys. Chem. A* **2000**, *104*, 7030.
(15) Choi, Y. M.; Park, J.; Lin, M. C. *J. Phys. Chem. A* **2003**, submitted.
(16) Nam, G.-J.; Xia, W.; Park, J.; Lin, M. C. *J. Phys. Chem. A* **2000**, *104*, 1233.
(17) Park, J.; Burova, S.; Rodgers, A. S.; Lin, M. C. *J. Phys. Chem. A* **1999**, *103*, 9036.
(18) Park, J.; Lin, M. C. *ACS Symp. Ser.* **1999**, *720*, 196.
(19) Park, J.; Gheyas, S. I.; Lin, M. C. *Int. J. Chem. Kinet.* **1999**, *31*, 645.
(20) Park, J.; Chakraborty, D.; Bhusari, D. M.; Lin, M. C. *J. Phys. Chem.* A **1999**, *103*, 4002.
(21) O'Keefe, A.; Deacon, D. A. *Rev. Sci. Instrum.* **1988**, *59*, 2544.
(22) Porter, G.; Ward, B. *Proc. R. Soc. Ser. A* **1965**, *287*, 457.
(23) Radziszewski, J. G. *Chem. Phys. Lett.* **1999**, *301*, 565.
(24) Johnson, R. P. *J. Org. Chem.* **1984**, *49*, 4857.
(25) Krauss, M.; Roszak, S. *J. Mol. Struct. (THEOCHEM)* **1994**, *116*, 155.
(26) Engert, J. M.; Dick, B. *Appl. Phys. B* **1996**, *B 63*, 531.
(27) Friderichsen, A. V.; Radziszewski, J. G.; Nimlos, M. R.; Winter, P. R.; Dayton, D. C.; David, D. E.; Ellison, G. B. *J. Am. Chem. Soc.* **2001**, *123*, 1977.
(28) Lapinski, A.; Spanget-Larsen, J.; Langgard, M.; Waluk, J.; Radziszewski, J. G. *J. Phys. Chem. A* **2001**, *105*, 10520.
(29) Radziszewski, J. G.; Nimlos, M. R.; Winter, P. R.; Ellison, G. B. *J. Am. Chem. Soc.* **1996**, *118*, 7400.
(30) Kim, G.-S.; Mebel, A. M.; Lin, S. H. *Chem. Phys. Lett.* **2002**, *361*, 421.
(31) Tonokura, K.; Norikane, Y.; Koshi, M.; Nakano, Y.; Nakamichi, S.; Goto, M.; Hashimoto, S.; Kawasaki, M.; Andersen Sulbaek, M. P.; Hurley, M. D.; Wallington, T. J. *J. Phys. Chem. A* **2002**, *106*, 5908.
(32) Xia, W. S.; Lin, M. C. *Phys. Chem. Chem. Phys.* **2000**, *2*, 5566.
(33) National Instruments, *LabVIEW User Manual*, 5.1, 1998.
(34) Frisch, M. J.; Trucks, G. W.; Schlegel, H. B.; Scuseria, G. E.; Robb, M. A.; Cheeseman, J. R.; Zakrzewski, V. G.; Montgomery, J. A., Jr.; Stratmann, R. E.; Burant, J. C.; Dapprich, S.; Millam, J. M.; Daniels, A. D.; Kudin, K. N.; Strain, M. C.; Farkas, O.; Tomasi, J.; Barone, V.; Cossi, M.; Cammi, R.; Mennucci, B.; Pomelli, C.; Adamo, C.; Clifford, S.; Ochterski, J.; Petersson, G. A.; Ayala, P. Y.; Cui, Q.; Morokuma, K.; Malick, D. K.; Rabuck, A. D.; Raghavachari, K.; Foresman, J. B.; Cioslowski, J.; Ortiz, J. V.; Stefanov, B. B.; Liu, G.; Liashenko, A.; Piskorz, P.; Komaromi, I.; Gomperts, R.; Martin, R. L.; Fox, D. J.; Keith, T.; Al-Laham, M. A.; Peng, C. Y.; Nanayakkara, A.; Gonzalez, C.; Challacombe, M.; Gill, P. M. W.; Johnson, B. G.; Chen, W.; Wong, M. W.; Andres, J. L.; Head-Gordon, M.; Replogle, E. S.; Pople, J. A. *Gaussian 98*, revision A.7; Gaussian, Inc.: Pittsburgh, PA, 1998.
(35) Becke, A. D. *J. Chem. Phys.* **1992**, *96*, 2155.
(36) Becke, A. D. *J. Chem. Phys.* **1992**, *97*, 9173.
(37) Becke, A. D. *J. Chem. Phys.* **1993**, *98*, 5648.
(38) Kendall, R. A.; Dunning, T. H., Jr.; Harrison, R. J. *J. Chem. Phys.* **1992**, *96*, 6796.
(39) Woon, D. E.; Dunning, T. H., Jr. *J. Chem. Phys.* **1993**, *98*, 1358.
(40) Peng, C.; Ayala, P. Y.; Schlegel, H. B.; Frisch, M. J. *J. Chem. Phys.* **1996**, *17*, 49.
(41) Peng, C.; Schlegel, H. B. *Israel J. Chem.* **1994**, *33*, 449.
(42) Gonzalez, C.; Schlegel, H. B. *J. Chem. Phys.* **1989**, *90*, 2154.
(43) Gonzalez, C.; Schlegel, H. B. *J. Phys. Chem.* **1990**, *94*, 5523.
(44) Cvetanovic, R. J.; Singleton, D. L.; Paraskevopoulos, G. *J. Phys. Chem.* **1979**, *83*, 50.
(45) Kee, R. J.; Rupley, F. M.; Miller, J. A. CHEMKIN−II: A FORTRAN Program Chemical Kinetics Package for the Analysis of Gas-Phase Chemical Kinetics. Sandia National Laboratory Report No. SAND 89-8009; Sandia National Laboratory: Livermore, CA, 1988.
(46) Corchado, J. C.; Chuang, Y.-Y.; Fast, P. L.; Villa, J.; Hu, W.-P.; Liu, Y.-P.; Lynch, G. C.; Nguyen, K. A.; Jackels, C. F.; Melissas, V. S.; Lynch, B. J.; Ivan Rossi; Coitino, E. L.; Ramos, A. F.; Steckler, R.; Garrett, B. C.; Isaacson, A. D.; Truhlar, D. G. P*OLYRATE*, 8.5.1, 2000.
(47) McQuarrie, D. A. S*tatistical Mechanics*; University Science Books: Saualito, CA, 2000.
(48) Shimanouchi, T. T*ables of Molecular Vibrational Frequencies*; National Bureau of Standards, 1972; Vol. 1.
(49) Chuang, Y.-Y.; Truhlar, D. G. J. *Chem. Phys.* **2000**, *112*, 1221.
(50) Truhlar, D. G. T*he Reaction Path in Chemistry: Current Approaches and Perspectives*; Kluwar Academic Publishers: The Netherlands, 1995.
(51) Baboul, A. G.; Schlegel, H. B. J. *Chem. Phys.* **1997**, 10*7*, 9413.
(52) Truhlar, D. G. J. *Comput. Chem.* **1991**, *12*, 266.
(53) Park, J.; Dyakov, I. V.; Mebel, A. M.; Lin, M. C. *J. Phys. Chem.* **1997**, *101*, 6043.